Amino Acids (2012) 43:267–277
DOI 10.1007/s00726-011-1070-4

ORIGINAL ARTICLE

Effect of double mutations K214/A–E215/Q of FRATide on GSK3β: insights from molecular dynamics simulation and normal mode analysis

Shao-Yong Lu · Yong-Jun Jiang · Jian-Wei Zou · Tian-Xing Wu

Received: 9 June 2011 / Accepted: 2 August 2011 / Published online: 13 September 2011

Abstract Glycogen synthase kinase 3β (GSK3β) is a multifunctional serine/threonine protein kinase that is involved in several biological processes including insulin and Wnt signaling pathways. The Wnt signaling via FRAT-mediated displacement of axin inhibits GSK3β activity toward non-primed substrates without affecting its activity toward primed substrates. Herein, molecular dynamics simulation, molecular mechanics generalized Born/surface area (MM_GBSA) calculation, and normal mode analysis are performed to explore the structural influence of the double mutations K214/A–E215/Q of FRATide on the GSK3β–FRATide complex. The results reveal that the priming phosphate-binding site, the primed substrate-binding site, the alignment of the critical active site residues in the ATP-binding site, as well as the periodic open–closed conformational change of the ATP-binding site, which are critical for the catalytic activity of GSK3β, are negligibly influenced in the mutated system compared with the wild-type (WT) system. This indicates that FRATide does not inhibit the GSK3β activity toward primed substrates. Additionally, MM_GBSA calculation indicates that the less energy-favorable GSK3β–FRATide complex is observed in the mutant than in the WT complex.

Keywords GSK3β · Wnt signaling · MD simulation · MM_GBSA · Normal mode analysis

Abbreviations

MD	Molecular dynamics
GSK3	Glycogen synthase kinase 3
GS	Glycogen synthase
APC	Adenomatous polyposis coil protein
FRAT	Advanced T-cell lymphomas protein
CDK2	Cyclin-dependent kinase 2
MAP	Mitogen-activated protein kinase
eIF2B	Eukaryotic initialization factor 2B
CREB	cAMP-responsive element-binding protein
Tau	Microtubule-binding protein
GBP	GSK3-binding protein
KE	Lysine and glutamic acid
AQ	Alanine and glutamine
NMA	Normal mode analysis
MM_GBSA	Molecular mechanics generalized born/surface area
PDB	Protein data bank
RMSD	Root mean-square deviation

Introduction

As a serine/threonine protein kinase, glycogen synthase kinase 3 (GSK3) is ubiquitously expressed in mammalian tissues (Emibi et al. 1980; Welsh and Proud 1993; Ali et al. 2001). In mammals, GSK3 is coded by two highly homologous isoforms, GSK3α (51 kDa) and GSK3β

Electronic supplementary material The online version of this article (doi:10.1007/s00726-011-1070-4) contains supplementary material, which is available to authorized users.

S.-Y. Lu · T.-X. Wu
Department of Chemistry, Zhejiang University, Hangzhou 310027, Zhejiang, China
e-mail: lushaoyong@yeah.net

Y.-J. Jiang (✉) · J.-W. Zou
Key Laboratory for Molecular Design and Nutrition Engineering, Ningbo Institute of Technology, Zhejiang University, Ningbo 315104, China
e-mail: yjjiang@nit.zju.edu.cn

(47 kDa) (Ali et al. 2001). The two genes share a sequence identity of 93% in their catalytic domains and exhibit similar biological functions, but mainly diverge at the N and C termini. Although GSK3 was originally identified in insulin signaling and metabolic regulation, later research has unequivocally ascertained that GSK3 is engaged in many signaling pathways including Wnt, NF-*k*B, Estradiol, and Reelin pathways (Grimes and Jope 2001; Doble and Woodgett 2003; Harwood 2001). An elevation or aberrant regulation of its normal activity level is associated with numerous disease states, including type 2 diabetes, cancer, Alzheimer's disease, Huntington's disease, bipolar disorder, and chronic inflammation (Ali et al. 2001; Eldar-Finkelman et al. 2010).

Unlike many other protein kinases, the autoinhibition of GSK3 is a hallmark of the phosphorylation of an N-terminal serine residue (Ser9 in GSK3β and Ser21 in GSK3α) via the PKB/AKT pathway (Cross et al. 1995). The phosphoserine, acting as a pseudosubstrate, occupies the same binding site as the priming phosphate of the substrate and blocks access to the catalytic site. This in turn results in activation of prephosphorylated (primed) substrates such as glycogen synthase (GS), thereby contributing to the stimulation of glycogen synthesis and subsequently modulating blood glucose levels. This is called insulin signaling, which is important for the treatment of diabetes. However, GSK3 activity toward non-primed substrates such as cytoplasmic β-catenin is not affected by this pathway. GSK3 activity can also be controlled by the canonical Wnt signaling pathway.

Wnt signaling pathway controls cell fate determination and cell renewal (Cadigan and Nusse 1997). It has been implicated in cancer, osteoporosis, and neurodegenerative disorders (Miller et al. 1999; Peifer and Polakis 2000). In the absence of a Wnt signal, GSK3 is involved in a multiprotein complex that contains axin and adenomatous polyposis coil protein (APC). Phosphorylation of β-catenin by GSK3 targets it for degradation via ubiquitin-dependent proteolysis (Aberle et al. 1997; Rubinfeld et al. 1996). In the activated Wnt signaling, the extracellular Wnt binds to the Frizzled/LRP transmembrane receptors. This initiates an intracellular signaling cascade consisting of Dishevelled (Dvl) and frequent rearrangement in advanced T-cell lymphomas (FRAT) proteins that lead to the inhibition of GSK3. In this process, FRAT competes with axin for binding to GSK3, resulting in disruption of the GSK3/axin/APC multiprotein complex and the formation of FRAT1/GSK3 complex, thereby preventing the phosphorylation and degradation of β-catenin, but not the phosphorylation of primed substrates (Chou et al. 2006; Hay et al. 2005; Thomas et al. 1999). As a result, unphosphorylated β-catenin accumulates in the cytoplasm and translocates to the nucleus, where it can activate members of the TCF/LEF transcription factors. The inappropriate activation of proliferative genes such as c-*myc* by the elevated β-catenin is associated with cancerogenesis. In essence, compared with the insulin signaling, Wnt signaling inhibits GSK3 activity toward non-primed substrates without affecting its activity toward primed substrates. Additionally, the primed and non-primed protein substrates of GSK3 are summarized in Table S1.

Compared with cyclin-dependent kinase 2 (CDK2), mitogen-activated protein kinase (MAP)/ERK2 and cAMP-dependent protein kinase (PKA), GSK3 has a unique specificity for its primed substrates, such as GS, eukaryotic initialization factor 2B (eIF2B), and cAMP-responsive element-binding protein (CREB). It prefers phosphorylation of its substrates at the P+4 serine [S(p)] before it can further phosphorylate the substrates at the P0 serine in the canonical motif SXXXS(p), where S(p) is the primed phosphorylation site. The P0 and the P+4 serines are separated by three residues. This is called primed phosphorylation mechanism and is $\sim$2–3 orders of magnitudes larger than phosphorylation without priming (Thomas et al. 1999). Recent computational studies from our group have evidenced that the primed substrate not only optimizes the proper orientation of the GSK3N- and C-terminal domains but also clamps the P0 serine of primed substrate in the appropriate configuration for interaction with the ATP γ-phosphate for the optimal phosphorylation reaction to occur (Lu et al. 2011a).

Experimentally, Thomas et al. (1999) have reported that FRATide (a peptide corresponding to residue 188–226 of FRAT1) selectively inhibits the GSK3-catalyzed phosphorylation of axin and β-catenin in vitro, but does not suppress GSK3 activity toward primed substrates derived from GS, eIF2B, and CREB. Furthermore, Culbert et al. (2001) demonstrated that cellular overexpression of FRAT1 correlates with inhibition of GSK3 activity toward microtubule-binding protein (Tau) and β-catenin, but not modulation of GS activity. Aside from these, GSK3-binding protein (GBP)/FRAT1 does not inhibit phosphorylation of a CREB-derived peptide substrate by GSK3, also supporting the notion that the nature of FRAT/GBP-mediated inhibition of GSK3 activity is selective (Farr III et al. 2000). Double mutations of the KE sequence to AQ in the *Xenopus* FRAT homolog, GBP, abolish GSK3 binding (Yost et al. 1998). Despite the extensive experimental observations, the mechanism for the selective inhibition of GSK3 activity by FRAT has not been rationalized at the atomic level.

Computational studies are increasingly gaining interest in elucidating the pathways connecting the active and inactive forms of the kinases and play an important

complementary role with respect to experiments (Buch et al. 2010; Tang et al. 2011; Lu et al. 2011b, c). Recently, we elucidate the allosteric regulation mechanism regarding mutation K85M of GSK3β on the GSK3β–FRATide complex via molecular dynamics (MD) simulation and normal mode analysis (NMA) (Lu et al. 2011d). The allosteric regulation originates form the observation that the mutation K85M at the N-terminal domain of GSK3β, in the ATP-binding site, not only inhibits GSK3β activity toward the phosphorylation of primed substrates, but also abolishes the binding of FRATide that binds at a distal site at the C-terminal domain, to GSK3β (Lu et al. 2011d).

In this study, we use MD simulation, molecular mechanics generalized Born/surface area (MM_GBSA) calculation, and NMA to investigate the structural influence of the double mutations K214/A–E215/Q of FRATide, in the FRATide-binding site, on the GSK3β–FRATide complex. Here, we aim to gain better understanding of the selective inhibition of GSK3 activity by FRATide. The obtained results may provide an insight into the different mechanisms in insulin and Wnt signaling pathways.

Materials and methods

Systems setup

To date, there are no crystal structures of GSK3α. Thus, GSK3β, the most structurally characterized kinase of the GSK3 family, is used. The initial 2.6 Å wild-type GSK3β–FRATide complex was extracted from the RCSB Protein Data Bank (PDB ID: 1GNG) (Bax et al. 2001). The construction of the double mutations K214/A–E215/Q of FRATide was carried out with the Biopolymer module of SYBYL 6.8 (Tripos Associates Inc.), using the crystallographic coordinates as a template and replacing target residues with the desired amino acids. The AMBER FF03 (Duan et al. 2003) force field was used for the GSK3β–FRATide complex. The force field parameters for the phosphorylated tyrosine 216 residue with a -2 (deprotonated) charge were obtained from the AMBER parameter database (Homeyer et al. 2006). All hydrogen atoms were added to the heavy atoms of the GSK3β–FRATide complex using the Xleap module in the AMBER 9 package (Case et al. 2006). Each system was embedded in the truncated octahedron box of the TIP3P (Jorgensen et al. 1983) water molecules with a 10.0 Å buffer. The eight Cl^- counter-ions were added to maintain the electroneutrality of each system. This was done by random substitution of water molecules with ions at the most favorable electrostatic potential positions. About 48,000 atoms were used for each system.

MD simulation

Energy minimizations and MD simulations were performed for each system using the SANDER module of the AMBER9 package. First, energy minimization of the water molecules and counter-ions with a positional restraint of 500 kcal/(mol Å^2) in the GSK3β–FRATide complex was performed to remove the bad contacts. Afterward, the whole system was minimized without any restraint. After relaxation, each system was gradually heated from 0 to 150 K, and then from 150 to 300 K in 10 ps. This was followed by constant temperature equilibration at 300 K for 300 ps, with a positional restraint of 10 kcal/(mol Å^2) in the GSK3β–FRATide complex in a canonical ensemble (NVT). Finally, 30 ns MD simulations were carried out on both systems in an isothermal isobaric ensemble (NPT) with periodic boundary conditions. An integration step of 2 fs was set for the MD simulations, and the long-range electrostatic interactions were treated by the particle mesh Ewald method (Darden et al. 1993), using a cubic fourth-order B-spline interpolation, and by setting the direct sum tolerance to 10^{-5}. A cutoff equal to 10 Å was used for short-range electrostatics and van der Waals interactions. The SHAKE method (Ryckaert et al. 1977), with a tolerance of 10^{-5} Å, was applied to constrain all covalent bonds involving hydrogen atoms. Each simulation was coupled to a 300 K thermal bath at 1.0 atm (1 atm = 101.3 kPa) by applying the Langevin algorithm (Wu and Brooks 2003). The temperature and pressure coupling parameters were set as 1.0 ps. The coordinates were saved every 1.0 ps for analysis.

MM_GBSA calculation

Energetic postprocessing was performed using the molecular mechanics generalized Born/surface area (MM_GBSA) method (Kollman et al. 2000; Hou et al. 2011a, b), which was used to calculate the relative free energies of substrate binding to GSK3β. The snapshots of each system were sampled from the last 1 ns with an interval of 10 ps. The binding free energies ($\Delta G_{\text{binding}}$) were calculated as follows:

$$\Delta G_{\text{binding}} = \Delta G_{\text{complex}} - \left[\Delta G_{\text{GSK3}\beta} + \Delta G_{\text{substrate}}\right] \quad (1)$$

$$\Delta G_{\text{binding}} = \Delta E_{\text{gas}} + \Delta G_{\text{solvation}} - T\Delta S \quad (2)$$

$$\Delta E_{\text{gas}} = \Delta E_{\text{vdW}} + \Delta E_{\text{ele}} + \Delta E_{\text{int}} \quad (3)$$

$$\Delta G_{\text{solvation}} = \Delta G_{GB} + \Delta G_{\text{nonpolar}} \quad (4)$$

$$\Delta G_{\text{nonpolar}} = \gamma \times \text{SASA} + \text{b}. \quad (5)$$

The sum of molecular mechanical energies, ΔE_{gas}, can be divided into contributions from van der Waals energy (ΔE_{vdW}), electrostatic energy (ΔE_{ele}), and internal energies

(ΔE_{int}) (Eq. 3). The solvation free energy, $\Delta G_{solvation}$, can be partitioned into two (Eq. 4): the polar contribution (ΔG_{GB}) and the nonpolar contribution ($\Delta G_{nonpolar}$). The polar contribution (ΔG_{GB}) to the solvation energy was calculated using the GB model (Onufriev's GB, IGB = 2). The dielectric constants used for the interior (solute) and exterior (water) were 1 and 80, respectively. Atomic radii and charges were the same as those used in the MD simulations. The nonpolar contributions ($\Delta G_{nonpolar}$) were calculated using the function of the solvent accessible surface area (SASA), which is determined using the linear combination of pairwise overlaps (Weiser et al. 1999); the probe radius was 1.4 Å, $\gamma = 0.0072$ kcal/(mol Å^2) and $b = 0$ kcal/mol (Eq. 5). The solute entropy contributions to the binding free energy, obtained from the sum of translational, rotational, and vibrational components, were not computed in this work because of the extremely long durations of NMA for large systems. Estimation of energies in this manner has proven successful in our previous studies (Lu et al. 2011a, d; Zhang et al. 2007, 2009; Sun et al. 2008).

Normal mode analysis (NMA)

The average structures obtained from the MD simulations for the two systems were used as the starting structure in a series of computational calculations. NMA was carried out using the web server of NOMAD-Ref developed by Lindahl et al. (2006) (http://lorentz.immstr.pasteur.fr/nomad-ref.php). During the NMA calculations, the single-parameter Hookean potential was used (Eq. 6).

$$E_p = \sum_{d_{ij}^0 < R_c} c(d_{ij} - d_{ij}^0)^2 \quad (6)$$

where d_{ij} is the distance between two atoms i and j, d_{ij}^0 is the distance between the atoms in the three-dimensional structure, c is a phenomenological constant assumed to be the same for all interacting pairs which refers to the spring constant of the potential, and R_c is an arbitrary cutoff parameter, beyond which interactions are not taken into account. In this study, R_c was set to be 10 Å. In both cases, the sparse metric solver method was used to calculate the lowest 25 modes. The first six trivial normal modes were discarded because they only represent translation and rotation.

Results and discussion

Global and local structural behavior

Conventional MD simulations of two systems, the wild-type (WT) and the double mutations K214/A–E215/Q of FRATide of the GSK3β–FRATide complexes were carried out in explicit water for 30 ns, respectively. The root mean-square deviation (RMSD) for all Cα atoms in relation to the X-ray crystal structure as a function of simulation time for the two simulated systems is shown in Fig. 1. This provides the first glimpse of any major conformational change that may have occurred during the MD simulations. The fluctuations of the complex follow the same trend in both cases throughout the simulations, and the RMSDs tend to converge at ~5 ns, with the RMSD values of 1.85 ± 0.22 and 1.83 ± 0.23 Å for the WT and the mutated systems, respectively. This indicates that the global structure of the complex remains quite similar to the initial one. The RMSD for the local structural domains in the two systems is tabulated in Table 1. In general, the loop domains show larger fluctuations compared with the helical domains. Inspection of Table 1 reveals that all domains in the two systems show a similar fluctuation except the second helical FRATide (residue 211–221), where it shows slightly larger fluctuation in the mutated system than in the WT complex, with the RMSD values of 1.23 ± 0.42 and 0.61 ± 0.15 Å for the mutant and the WT systems, respectively. This different fluctuation is reasonable because the positions of the double mutations K214/A–E215/Q of FRATide are located in the second helical FRATide.

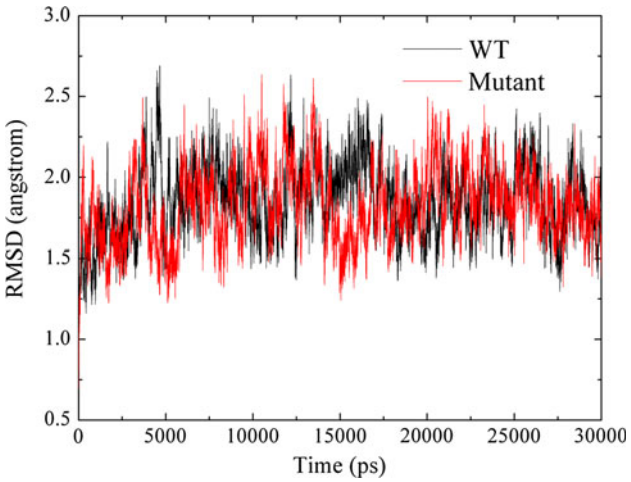

Fig. 1 The time dependence of RMSDs for the Cα atoms of the GSK3β–FRATide complex for the WT system (*black*) and the mutated systems (*red*) in the 30-ns MD simulations (color figure online)

Priming phosphate-binding site and primed substrate-binding site

In protein kinases, P38γ (Bellon et al. 1999), CDK2 (Brown et al. 1999), and PKA (Zheng et al. 1999), the phosphothreonine residues (p-Thr183 for P38γ, p-Thr160 for CDK2, and p-Thr197 for PKA) at the activation loop

Table 1 Root mean-square deviation (RMSD, Å) of structural domains of GSK3β–FRATide complex in the two simulated systems

Structural domains	WT	Mutant
N-lobe (36–138)	1.06 ± 0.13	1.08 ± 0.16
Helix D (139–149)	0.45 ± 0.17	0.35 ± 0.11
Helix E (155–174)	0.46 ± 0.08	0.40 ± 0.07
Helix F (237–252)	0.41 ± 0.07	0.42 ± 0.07
Helix G (262–273)	0.46 ± 0.11	0.37 ± 0.09
Helix H (278–284)	0.28 ± 0.08	0.25 ± 0.08
Helix I (311–321)	0.32 ± 0.07	0.34 ± 0.07
Loop 1 (150–154)	0.43 ± 0.15	0.41 ± 0.13
Loop 2 (175–236)	1.27 ± 0.32	1.31 ± 0.36
Loop 3 (253–261)	0.64 ± 0.14	0.52 ± 0.15
Loop 4 (274–277)	0.23 ± 0.09	0.20 ± 0.08
Loop 5 (285–300)	1.03 ± 0.19	1.10 ± 0.15
Loop 6 (301–310)	0.68 ± 0.22	0.59 ± 0.21
Irregular domain (322–385)	1.18 ± 0.23	1.19 ± 0.23
a1 helical FRATide (199–209)	0.46 ± 0.16	0.43 ± 0.17
a2 helical FRATide (211–221)	0.61 ± 0.15	1.23 ± 0.42

(A loop) appear to induce the active conformation of this loop for optimal catalytic activity. However, GSK3β does not have the threonine phosphorylation site in the A loop. Therefore, GSK3β uses the prephosphorylated serine residue at the P+4 position of the substrates to occupy the priming phosphate-binding site for the proper alignment of the N- and C-terminal domains for optimal catalytic activity (Lu et al. 2011a; ter Haar et al. 2001). The priming phosphate-binding site consists of three positively charged residues: Arg96, Arg180, and Lys205. Mutation of the triad or disruption of the interactions between the priming phosphate group of the substrate and the triad prevents phosphorylation of GSK3β primed substrates, a suggestion that finds support in results from experimental observations (Frame et al. 2011; Dajani et al. 2001) and computational studies (Zhang et al. 2009). Thus, whether the double mutations K214/A–E215/Q of FRATide would affect the dynamic behavior of the priming phosphate-binding site is explored. The average structures are calculated by averaging coordinates from the 30 ns collective trajectories. Figure 2 shows the superimposition of the backbone atoms of the average structures for the two systems. The priming phosphate-binding site is similar in the two systems, suggesting that the mutation scarcely influences the priming phosphate-binding site.

In GSK3β, the primed substrate-binding site is situated between the two lobes of the kinase domain. The FRATide-binding site or non-primed substrate-binding site is located on the C-terminal lobe of the kinase domain. Figure 3 illustrates the molecular surface visualizations of the two average structures. Clearly, the FRATide-binding site does not interfere with the primed substrate-binding site. The primed substrate-binding site is similar in the two systems; this indicates that the mutation has hardly any influence on the primed substrate-binding site.

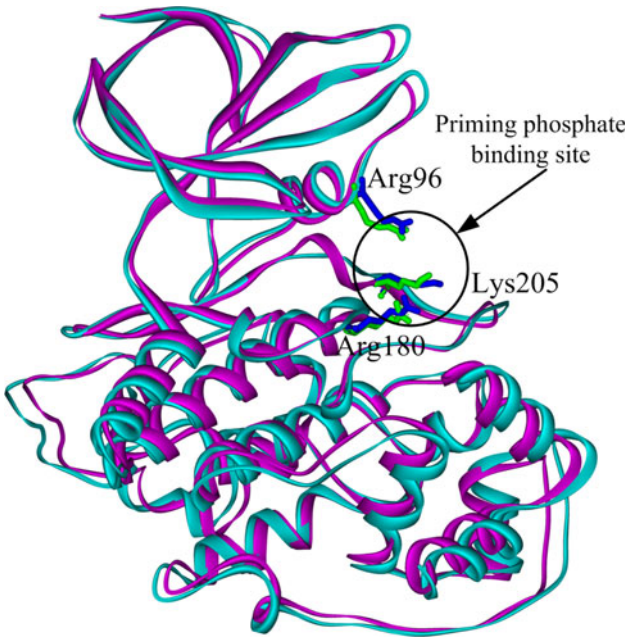

Fig. 2 The superimposition of the backbone atoms of the average structure of the GSK3β-FRATide complex between the WT (*cyan*) and the mutated systems (*magenta*). The three positively charged residues, Arg96, Arg180, and Lys205, consisting of the priming phosphate-binding site, are shown in stick for the WT (*green*) and the mutated systems (*blue*) (color figure online)

ATP-binding site and dynamics behavior of ATP-binding site

In GSK3β, the ATP-binding site is at the interface of the β-stranded domains and α-helical domains and is bordered by the G loop and the hinge domain. ATP active site residues contain Lys85, Asp133, Val135, Asp181, Lys183, Asn186, and Asp200. These residues help the ATP molecule to adopt an active conformation for the transfer of γ-phosphate group from ATP to a serine or threonine residues of GSK3β substrates. As shown in Fig. 4, the superimposition of the ATP active site residues between the average structures of the WT and the mutated systems reveals that the orientations of these residues are similar, with the RMSD value of 0.43 Å.

As previously reported (Lu et al. 2011d), the periodic open–closed conformational change of the ATP-binding site is critical for the function of the protein kinase. The K85M mutation of GSK3β on the GSK3β–FRATide complex results in the G loop to collapse into the ATP-binding site. This in turn prevents the ATP from binding to GSK3β (Raaf et al. 2009). Thus, we want to investigate

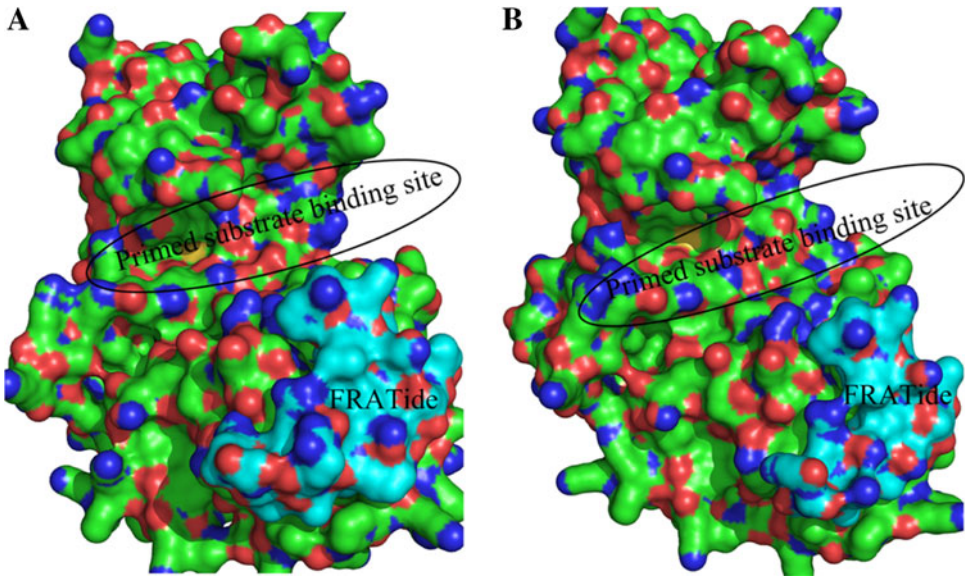

Fig. 3 Molecular surface visualizations of the two average structures for the WT (**a**) and the mutated systems (**b**)

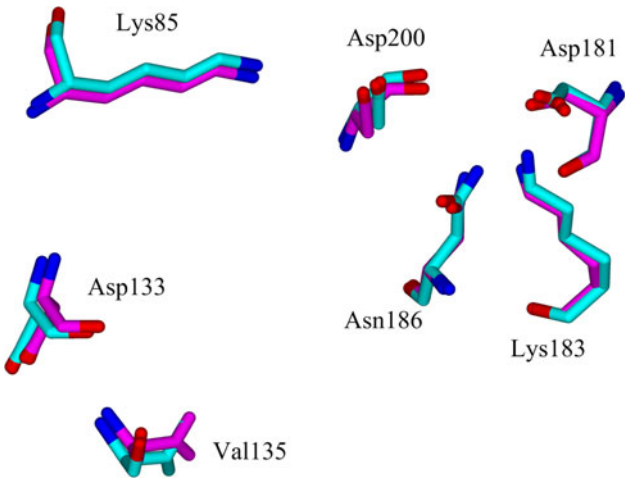

Fig. 4 The superimposition of the ATP active site residues between the average structures of the WT (carbon atoms colored in *cyan*) and the mutated systems (carbon atoms colored in *magenta*) (color figure online)

whether the double mutations K214/A–E215/Q of FRATide would affect the dynamic behavior of the ATP-binding site. Accordingly, the distance between the Ser66 at the tip of the G loop and the Asn186 beneath the triphosphate arm of ATP is monitored. This distance serves as the width of the entrance. As shown in Fig. 5, taking the mutated system as an example, the closed event of the ATP-binding site is at ~2,270 ps, correlating to the changes in the Ser66–Asn186 pairing distance. Then, the ATP-binding site gradually opens at ~3,200 ps, and the separation between Ser66 and Asn186 increases to a local maximum. As the simulation processes, the ATP-binding site gradually closes at ~5,000 ps, and the separation between Ser66 and Asn186 decreases to a local minimum. Afterward, it opens again at ~6,400 ps. The molecular surface visualizations of the open–closed process of the ATP-binding site in the mutated system as observed from MD simulations are shown in Fig. 6. Also, Fig. 7 shows the molecular surface visualizations of the open–closed process of the ATP-binding site in the WT system. This periodic open–closed conformational change of the ATP-binding site in the mutated system is similar to the WT system, as demonstrated in Figs. 6 and 7. This indicates that the mutant negligibly influences the dynamics behavior of the ATP-binding site.

As a complementary method to MD simulation, NMA is efficient for predicting large conformational changes in biological macromolecules. Thus, NMA is employed to study the opening and closing of the ATP-binding site of the GSK3β–FRATide complex. NMA reveals the concerted rocking of the N- and C-terminal domains of GSK3β, resulting in the opening and closing of the ATP-binding site, as shown in Videos S2 (WT) and S3 (Mutant). Obviously, The ATP-binding site in the mutated system opens or closes to a similar extent as the WT system, in good agreement with the dynamics behavior of the ATP-binding site in the MD simulations.

Hydrogen bonding interactions analysis

The FRATide consists of two amphipathic α-helices, α1 (residue 199–209) and α2 (residue 211–221). It adopts a helix–turn–helix conformation that packs against at the C-terminal domain of GSK3β mediated by hydrophobic and electrostatic interactions. The major GSK3β–FRATide interactions come from the α-helix (residue 267–273) and the extended loop (residue 285–299) of GSK3β and the α2-helix of FRATide. Residues Lys214 and Glu215 reside in

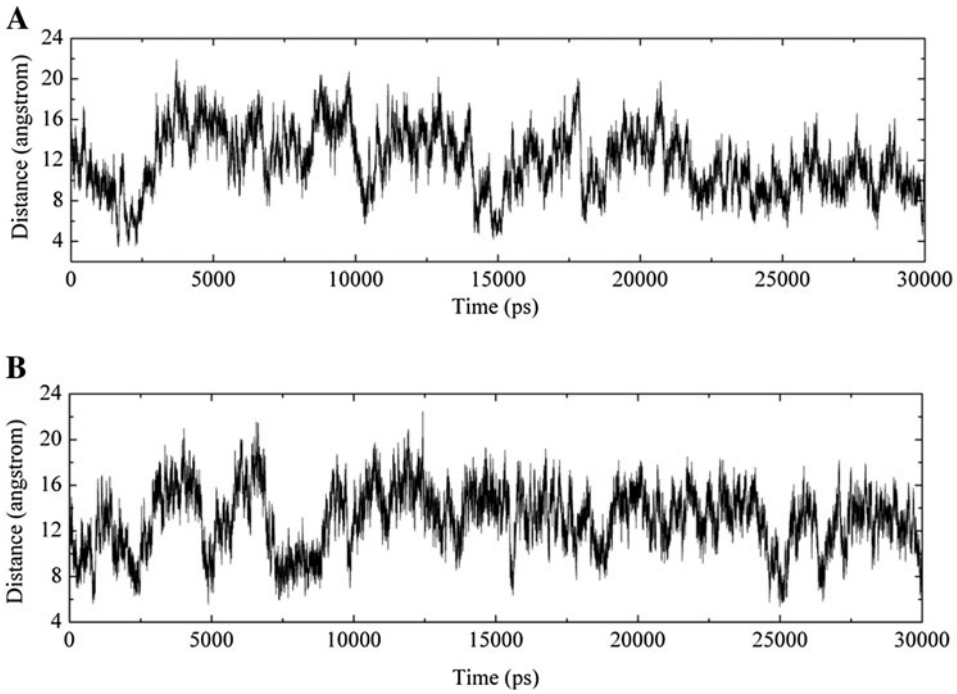

Fig. 5 The time dependence of the distance between the oxygen atom OG of Ser66 and the oxygen atom OD1 of Asn186 in the WT (**a**) and the mutated systems (**b**)

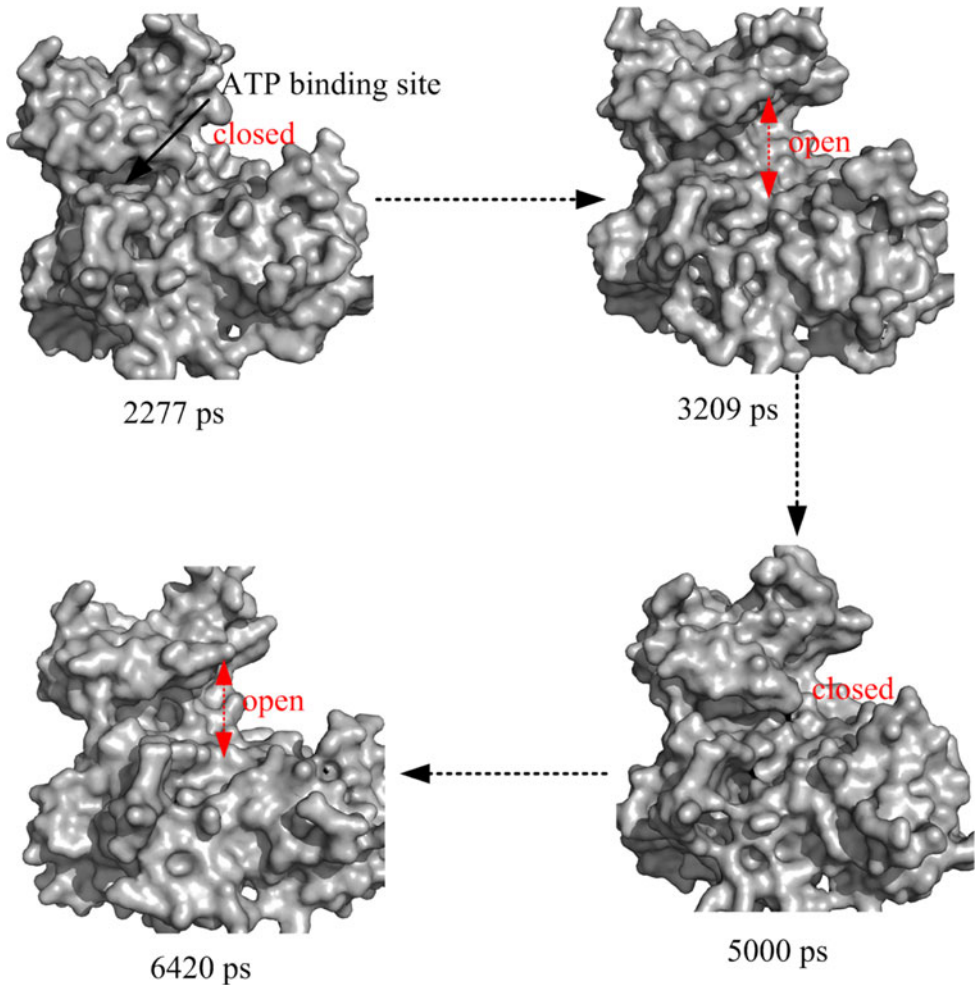

Fig. 6 Molecular surface visualizations of representative conformations of the mutated systems during the open–closed process of the ATP-binding site as observed from MD simulations. A *double dashed line* shows the ATP-binding site opening

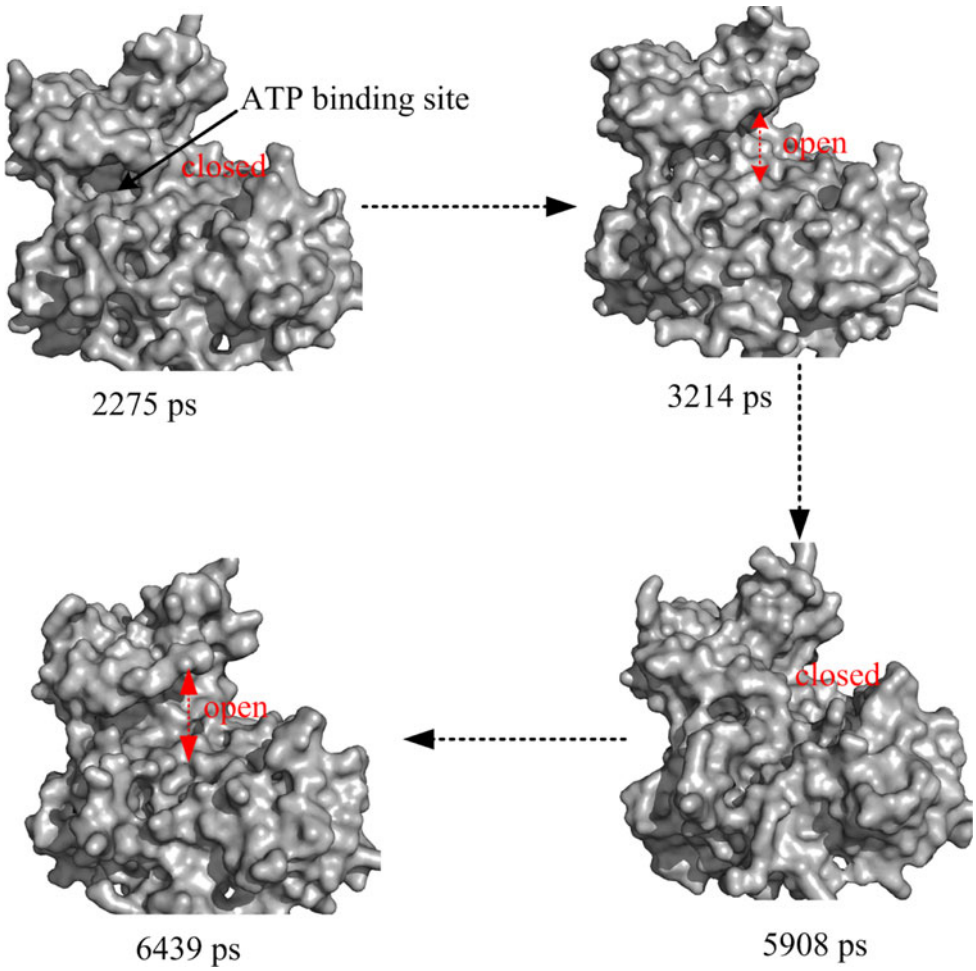

Fig. 7 Molecular surface visualizations of representative conformations of the WT systems during the open–closed process of the ATP-binding site as observed from MD simulations. A *double dashed line* shows the ATP-binding site opening

the α2-helix of FRATide. As observed in X-ray crystal structure (Bax et al. 2001), the main-chain N–H group of Lys214 donates a hydrogen bond to the side chain oxygen atom (OE1) of Glu290 from GSK3β. On the other hand, the side chain nitrogen atom (NZ) of Lys214 partakes in the hydrogen bonding interactions with the side chain oxygen atom (OE1) of Glu290 and with the main-chain oxygen atom of Lys292 from GSK3β. Additionally, the main-chain N–H groups of Leu212 and Ile213 from FRATide are hydrogen bonded to the side chain oxygen atoms from the Tyr288 OH and Glu290 OE2 atoms of GSK3β, respectively. The residue Glu215, which is solvent exposed, does not interact with GSK3β but involves in intra-hydrogen bonding or salt bridges interactions with Arg218 and Arg219 of FRATide. Therefore, the inter-hydrogen bonding interactions between GSK3β and FRATide as well as the intra-hydrogen bonding interactions in FRATide between Glu215 and Arg218 and Arg219 in the two simulated systems are analyzed.

The inter-hydrogen bonding interactions between GSK3β and FRATide characterized by means of average distances between heavy atoms and percentage of occurrence data are listed in Table 2. The observed inter-hydrogen bonding interactions in the crystal structure are conserved during the MD simulation in the WT system. However, due to the K214/A mutation in FRATide, the two

Table 2 Summary of the average distances between heavy atoms (Å) and percentage of occurrence data for inter-hydrogen bonding interactions between GSK3β and FRATide in the two systems

Hydrogen bond	WT		Mutant	
	X···Y	%	X···Y	%
Leu212-N–H···OH-Tyr288	3.14 ± 0.17	64.12	3.19 ± 0.17	82.40
Ile213-N–H···OE2-Glu290	2.84 ± 0.11	99.99	2.83 ± 0.10	100
Lys(Ala)214-N–H···OE1-Glu290	3.17 ± 0.15	92.11	2.95 ± 0.14	93.11
Lys214-NZ-HZ···OE1-Glu290	2.78 ± 0.11	99.75	–	–
Lys214-NZ-HZ···O-Lys292	2.88 ± 0.14	90.10	–	–

Table 3 Summary of the average distances between heavy atoms (Å) and percentage of occurrence data for intra-hydrogen bonding interactions between FRATide Glu(Gln)215 and FRATide Arg218 and FRATide Arg219 in the two systems

Hydrogen bond	WT		Mutant	
	X···Y	%	X···Y	%
Glu(Gln)215-OE1···HE–NE-Arg218	2.98 ± 0.21	71.09	2.99 ± 0.19	26.92
Glu(Gln)215-OE1···HH-NH2-Arg218	2.94 ± 0.25	68.61	2.94 ± 0.19	16.08
Glu215-OE2···HE–NE-Arg218	2.88 ± 0.14	59.58	–	–
Glu215-OE2···HH-NH2-Arg218	2.91 ± 0.22	81.06	–	–
Glu215-OE2(Gln215-OE1)···HE–NE-Arg219	3.04 ± 0.24	56.27	2.98 ± 0.19	16.40

hydrogen bonds (Lys214-NZ-HZ···OE1-Glu290 and Lys214-NZ-HZ···O-Lys290) are no longer formed in the mutated system. The loss of the two important hydrogen bonds is sufficient to eliminate binding with FRATide, as reported in experimental observations (Fraser et al. 2002; Dajani et al. 2003) and in our previous MD simulations (Lu et al. 2011d).

Table 3 summarizes the intra-hydrogen bonding interactions between FRATide Glu215 and FRATide Arg218, as well as FRATide Arg219. Specifically, in the WT complex, the side chain OE1 atoms of Glu215 form bifurcated hydrogen bonds (2.98 ± 0.21 Å, 71.09% occurrence and 2.94 ± 0.25 Å, 68.61% occurrence, respectively) with the side chain nitrogen atoms NE and NH2 of Arg218. The side chain OE2 atoms of Glu215 form trifurcated hydrogen bonds (2.88 ± 0.14 Å, 59.58% occurrence, 2.91 ± 0.22 Å, 81.06% occurrence, and 3.04 ± 0.24 Å, 56.27% occurrence, respectively) with the side chain nitrogen atoms, NE and NH2 of Arg218 and with the side chain nitrogen atom NE of Arg219 (Fig. 8a). In contrast, in the mutated system, the intra-hydrogen bonding interactions cannot form between Gln215 and Arg218 and Arg219, as evidenced in the hydrogen bonding occurrence data. This leads to movement of the side chains of Gln215, Arg218, and Arg219 away from their initial positions (Fig. 8b) and subsequently may lose the helical conformation. In contrast, in WT, these intra-hydrogen bonds constrain the side chain of Glu215, Arg218, and Arg219 in a compact conformation.

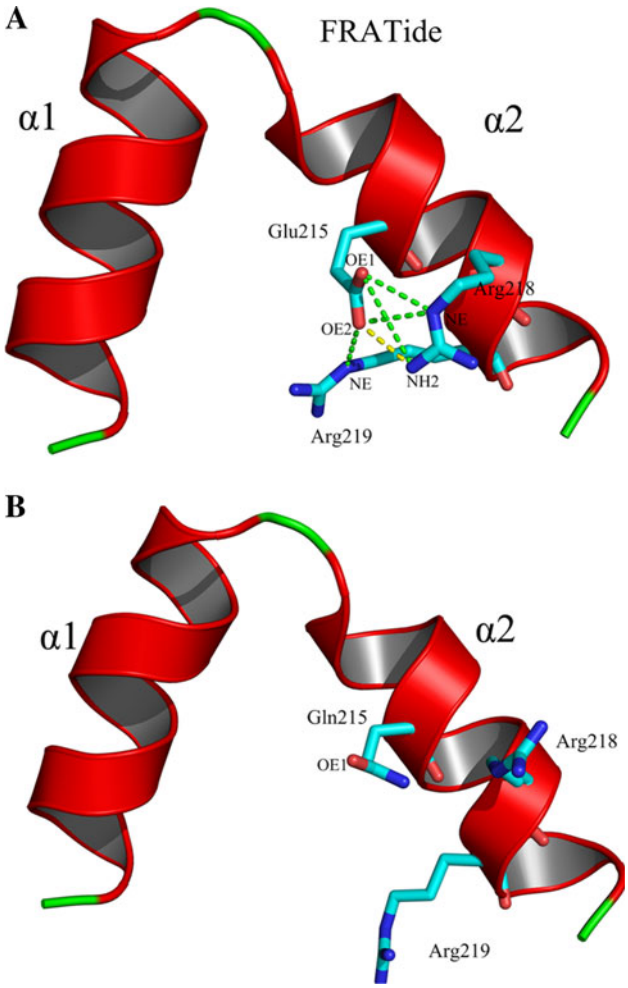

Fig. 8 The side chain conformations of Glu(Gln)215, Arg218, and Arg219 from the α2 helical FRATide for the WT (**a**) and the mutated systems (**b**)

Binding free energy calculations

To obtain further information of the contributions of energy component to the GSK3β–FRATide interaction in the WT and mutated systems, various components of the binding free energy ($\Delta G_{binding}$) of the complex are evaluated using the MM_GBSA method. Table 4 shows the decomposition of energy terms and the $\Delta G_{binding}$ of GSK3β–FRATide. According to the components of the $\Delta G_{binding}$, the favorable formation of the GSK3β–FRATide complex is driven by the electrostatic (ΔE_{ele}) and the van der Walls (ΔE_{vdW}) terms of the molecular mechanics energy and the nonpolar component of the solvation energy ($\Delta G_{nonpolar}$). The total electrostatic interaction (ΔG_{ele}) between the GSK3β and FRATide, which are composed of the gas phase ΔE_{ele} and the polar solvation free energy contributions (ΔG_{GB}), in the mutated system is ~14 kcal/mol less favorable than that of the WT system. This is in accordance with less hydrogen bonding interactions between GSK3β and FRATide in the mutated systems. The intermolecular ΔE_{vdW} and the nonpolar contributions ($\Delta G_{nonpolar}$) of the mutated system are ~8 kcal/mol less

Table 4 Energy terms of the binding free energy of the WT and the mutated systems (kcal/mol)

Energy terms	WT[a]		Mutant	
	Mean	SD	Mean	SD
ΔE_{ele}^{b}	−191.41	19.37	−104.87	18.32
ΔE_{vdW}^{c}	−97.70	5.09	−89.59	5.70
ΔE_{gas}^{d}	−289.11	19.90	−194.46	18.70
ΔG_{np}^{e}	−13.57	0.34	−12.80	0.51
ΔG_{gb}^{f}	216.12	18.13	143.51	18.20
ΔG_{sol}^{g}	202.55	18.04	130.71	18.65
ΔG_{ele}^{h}	24.71	5.34	38.64	4.40
$\Delta G_{binding}^{i}$	−86.41	5.40	−63.75	3.78
$\Delta\Delta G_{binding}^{j}$	0		22.66	

$\Delta E_{gas} = \Delta E_{ele} + \Delta E_{vdW}$, $\Delta G_{sol} = \Delta G_{np} + \Delta G_{gb}$, $\Delta G_{ele} = \Delta E_{ele} + \Delta G_{gb}$, $\Delta G_{binding} = \Delta E_{gas} + \Delta G_{sol}$

[a] The values were taken from Lu et al. (2011d)

[b] ΔE_{ele} is the electrostatic energy calculated by the MM force field

[c] ΔE_{vdW} is van der Waals contribution from MM force field

[d] ΔE_{gas} is absolute free energy in the gas phase

[e] ΔG_{np} is nonpolar contribution to the solvation free energy

[f] ΔG_{gb} is polar contribution to the solvation free energy calculated

[g] ΔG_{sol} is solvation free energy

[h] ΔG_{ele} is total electrostatic energy contribution to the binding energy

[i] $\Delta G_{binding}$ is the binding energy

[j] $\Delta\Delta G_{binding}$ is the value relative to the WT

favorable than that of the WT system. The total $\Delta G_{binding}$ in the mutated system is ~22 kcal/mol higher than that of the WT system. This means that the mutated system yields a less energy-favorable complex that subsequently would lead to the non-binding of the FRATide to GSK3β, consistent with the experimental studies (Yost et al. 1998). As a result, axin could bind to GSK3β and phosphorylation of β-catenin by GSK3β, targeting it for degradation, could be conducted. The Wnt signaling via FRAT-mediated displacement of axin could be inhibited, which could be potentially useful in some human cancers (Bax et al. 2001).

Conclusions

MD simulation, MM_GBSA-binding energy calculation, and NMA are employed to explore the effect of the double mutations K214/A–E215/Q of FRATide on GSK3β. The priming phosphate-binding site composed of three positively charged residues, Arg96, Arg180, and Lys205, the primed substrate-binding site, the alignment of the critical residues (Lys85, Asp133, Val135, Asp181, Lys183, Asn186, and Asp200) in the ATP-binding site, as well as the periodic open–closed conformational change of the ATP-binding site are similar in the WT and in the mutated systems. Thus, double mutations of the FRATide do not affect the GSK3β activity toward the primed substrates. Binding free energy calculation provides a qualitative explanation of the energetic effects of double mutations of FRATide on the binding affinity between GSK3β and FRATide. The mutated system could lead to a less energy-favorable GSK3β–FRATide complex, which would lead to the non-binding of the FRATide to GSK3β. The computational results, complementary to the experiments, may explain the selective inhibition of GSK3 activity by FRATide.

Acknowledgments This work was supported by the Natural Science Foundation of China (No.20803063).

References

Aberle H, Bauer A, Stappert J, Kispert A, Kemler R (1997) β-catenin is a target for the ubiquitin–proteasome pathway. EMBO J 16:3797–3804

Ali A, Hoeflich KP, Woodgett JR (2001) Glycogen synthase kinase-3: properties, functions, and regulation. Chem Rev 101:2527–2540

Bax B, Carter PS, Lewis C, Guy AR, Bridges A, Tanner R, Pettman G, Mannix C, Culbert AA, Brown MJB, Smith DG, Reith AD (2001) The structure of phosphorylated GSK-3β complexed with a peptide, FRATide, that inhibits β-catenin phosphorylation. Structure 9:1143–1152

Bellon S, Fitzgibbon MJ, Fox T, Hsiao HM, Wilson KP (1999) The structure of phosphorylated P38γ is monomeric and reveals a conserved activation-loop conformation. Structure 7:1057–1065

Brown NR, Noble MEM, Endicott JA (1999) The structural basis for specificity of substrate and recruitment peptides for cyclin-dependent kinases. Nat Cell Biol 1:438–443

Buch I, Fishelovitch D, London N, Raveh B, Wolfson HJ, Nussinov R (2010) Allosteric regulation of glycogen synthase kinase 3β: a theoretical study. Biochemistry 49:10890–10901

Cadigan KM, Nusse R (1997) Wnt signaling: a common theme in animal development. Genes Dev 11:3286–3305

Case DA, Darden TA, Cheatham TE III, Simmerling C, Wang J, Duke RE, Luo R, Merz KM, Pearlman DA, Crowley M, Walker RC, Zhang B, Wang S, Hayik A, Roitberg G, Seabra KF, Wong F, Paesani X, Wu S, Brozell V, Tsui H, Gohlke L, Yang C, Tan J, Mongan V, Hornak G, Cui P, Beroza DH, Mathews C, Schafmeister WSR, Kollman PA (2006) AMBER 9, University of California, San Francisco

Chou HY, Howng SL, Cheng TS, Hsiao YL, Lieu AS, Loh JK, Hwang SL, Lin CC, Hsu CM, Wang C, Lee CI, Lu PJ, Chou CK, Huang CY, Hong YR (2006) GSKIP is homologous to the Axin GSK3β interaction domain and functions as a negative regulator of GSK3β. Biochemistry 45:11379–11389

Cross DAE, Alessi DR, Cohen P, Andjelkovich M, Hemmings BA (1995) Inhibition of glycogen synthase kinase-3 by insulin mediated by protein kinase B. Nature 378:785–789

Culbert AA, Brown MJ, Frame S, Hagen T, Cross DAE, Bax B, Reith AD (2001) GSK-3β inhibition by adenoviral FRAT1 overexpression is neuroprotective and induces Tau phosphorylation and β-catenin stabilization without elevation of glycogen synthase activity. FEBS Lett 507:288–294

Dajani R, Fraser E, Roe SM, Young N, Good V, Dale TC, Pearl LH (2001) Crystal structure of glycogen synthase kinase 3β:

structural basis for phosphate-primed substrate specificity and autoinhibition. Cell 105:721–732

Dajani R, Fraser E, Roe SM, Maggie Y, Good VM, Thompson V, Dale TC, Pearl LH (2003) Structural basis for recruitment of glycogen synthase kinase 3β to the axin–APC scaffold complex. EMBO J 22:494–501

Darden T, York D, Pedersen L (1993) Particle mesh Ewald: an N log(N) method for Ewald sums in large systems. J Chem Phys 98:10089–10094

Doble BW, Woodgett JR (2003) GSK-3: tricks of the trade for a multi-tasking kinase. J Cell Sci 116:1175–1186

Duan Y, Wu C, Chowdhury S, Lee MC, Xiong G, Zhang W, Yang R, Cieplak P, Luo R, Lee T (2003) A point-charge force field for molecular mechanics simulations of proteins. J Comput Chem 24:1999–2012

Eldar-Finkelman H, Licht-Murava A, Pietrokovaski S, Eisenstein M (2010) Substrate-competitive GSK-3 inhibitors—strategy and implications. Biochim Biophys Acta 1804:598–603

Emibi N, Rylatt DB, Cohen P (1980) Glycogen synthase kinase-3 form rabbit skeletal muscle: separation from cylic-AMP-dependent protein kinase and phosphorylase kinase. Eur J Biochem 107:519–527

Farr GH III, Ferkey DM, Yost C, Pierce SB, Weaver C, Kimelman D (2000) Interaction among GSK-3, GBP, Axin, and APC in Xenopus axis specification. J Cell Biol 148:691–701

Frame S, Cohen P, Biondi RM (2001) A common phosphate binding site explains the unique substrate specificity of GSK3 and its inactivation by phosphorylation. Mol Cell 7:1321–1327

Fraser E, Young N, Dajani R, Franca-Koh J, Ryves J, Williams RSB, Yeo M, Webster MT, Richardson C, Smalley MJ, Pearl LH, Harwood A, Dale TC (2002) Identification of the Axin and Frat binding region of glycogen synthase kinase-3. J Biol Chem 277:2176–2185

Grimes GA, Jope RS (2001) The multifaceted roles of glycogen synthasekinase 3βin cellular signaling. Prog Neurobiol 65:391–426

Harwood AJ (2001) Regulation of GSK-3: a cellular multiprocessor. Cell 105:821–824

Hay E, Faucheu C, Suc-Royer I, Touitou R, Stiot V, Vayssiere B, Baron R, Roman–Roman S, Rawadi G (2005) Interaction between LRP5 and Frat1 mediates the activation of the Wnt canonical pathway. J Biol Chem 280:13616–13623

Homeyer N, Horn AH, Lanig H, Sticht H (2006) AMBER force field parameters for phosphorylated amino acids in different protonation states: phosphoserine, phosphothreonine, phosphotyrosine and phosphohistidine. J Mol Model 12:281–289

Hou T, Wang J, Li Y, Wang W (2011a) Assessing the performance of the MM/PBSA and MM/GBSA methods. 1. The accuracy of binding free energy calculations based on molecular dynamics simulations. J Chem Inf Model 51:69–82

Hou T, Wang J, Li Y, Wang W (2011b) Assessing the performance of the molecular mechanics/Poisson Boltzmann surface area and molecular mechanics/generalized Born surface area method. II: the accuracy of ranking poses generated from docking. J Comput Chem 32:866–877

Jorgensen WL, Chandrasekhar J, Madura JD, Impey RW, Klein ML (1983) Comparison of single potential function for simulating liquid water. J Chem Phys 79:926–935

Kollman PA, Massova I, Reyes C, Kuhn B, Shuanghong H, Chong L, Case DA (2000) Cheatham TEIII Calculating structures and free energies of complex molecules: combining molecular mechanics and continuum models. Acc Chem Res 33:889–897

Lindahl E, Azuara C, Koehl P, Delarue M (2006) NOMAD-Ref: visualization, deformation and refinement of macromolecular structures based on all-atom normal mode analysis. Nucleic Acids Res 34:W52–W56

Lu SY, Jiang YJ, Zou JW, Wu TX (2011a) Molecular modeling and molecular dynamics simulation studies of the GSK3β/ATP/substrate complex: understanding the unique P+4 primed phosphorylation specificity for GSK3β substrates. J Chem Inf Model 51:1025–1036

Lu SY, Jiang YJ, Lv J, Zou JW, Wu TX (2011b) Role of bridging water molecules in GSK3β-inhibitor complexes: insights from QM/MM, MD, and molecular docking studies. J Comput Chem 32:1907–1918

Lu SY, Jiang YJ, Zou JW, Wu TX (2011c) Dissection of the difference between the group I metal ions in inhibiting GSK3β: a computational study. Phys Chem Chem Phys 13:7014–7023

Lu SY, Jiang YJ, Lv J, Zou JW, Wu TX (2011d) Mechanism of kinase inactivation and nonbinding of FRATide to GSK3β due to K85M mutation: molecular dynamics simulation and normal mode analysis. Biopolymers 95:669–681

Miller JR, Hocking AM, Brown JD, Moon RT (1999) Mechanism and function of signal transduction by the Wnt/beta-catenin and Wnt/Ca^{2+} pathways. Oncogene 18:7860–7872

Peifer M, Polakis P (2000) Wnt signaling in oncogenesis and embryogenesis—a look outside the nucleus. Science 287: 1606–1609

Raaf J, Issinger OG, Niefind K (2009) First inactive conformation of CK2α, the catalytic subunit of protein kinase CK2. J Mol Biol 386:1212–1221

Rubinfeld B, Albert I, Porfiri E, Fiol C, Munemitsu S, Polakis P (1996) Binding of GSK3β to the APC-β–catenin complex and regulation of complex assembly. Science 272:1023–1026

Ryckaert JP, Ciccotti G, Berendsen HJC (1977) Numerical integration of the cartesian equations of motion of a system with constraints: molecular dynamics of n-alkanes. J Comput Phys 23:327–341

Sun H, Jiang YJ, Yu QS, Luo CC, Zou JW (2008) Effect of mutation K85R on GSK3β: molecular dynamics simulation. Biochem Biophys Res Commun 377:962–965

Tang XN, Lo CW, Chuang YC, Chen CT, Sun YC, Hong YR, Yang CN (2011) Prediction of the binding mode between GSK3β and a peptide derived from GSKIP using molecular dynamics simulation. Biopolymers 95:461–471

ter Haar E, Coll JT, Austen DA, Hsiao HM, Swenson L, Jain J (2001) Structure of GSK3β reveals a primed phosphorylation mechanism. Nat Struct Biol 8:593–596

Thomas GM, Frame S, Goedert M, Nathke I, Polakis P, Cohen P (1999) A GSK3-binding peptide from FRAT1 selectively inhibits the GSK3-catalysed phosphorylation of Axin and β-catenin. FEBS Lett 458:247–251

Weiser J, Shenkin PS, Still WC (1999) Approximate atomic surfaces from linear combinations of pairwise overlaps (LCPO). J Comput Chem 20:217–230

Welsh GI, Proud CG (1993) Glycogen synthase kinase-3 is rapidly inactivated in response to insulin and phosphorylates eukaryotic initiation factor eIF-2B. Biochem J 294:625–629

Wu X, Brooks BR (2003) Self-guided Langevin dynamics simulation method. Chem Phys Lett 381:512–518

Yost C, Farr GH III, Pierce SB, Ferkey DM, Chen MM, Kimelman D (1998) GBP, an inhibitor of GSK-3, is implicated in Xenopus development and oncogenesis. Cell 93:1031–1041

Zhang N, Jiang Y, Zou J, Zhuang S, Jin H, Yu Q (2007) Insights into unbinding mechanisms upon two mutations investigated by molecular dynamics study of GSK-3β–Axin complexes: role of packing hydrophobic residues. Proteins 67:941–949

Zhang N, Jiang Y, Zou J, Yu Q, Zhao W (2009) Structural basis for the complete loss of GSK3β catalytic activity due to R96 mutation investigated by molecular dynamics study. Proteins 75:671–681

Zheng J, Knighton DR, Teneyck LF, Karlsson R, Xuong NH, Taylor SS, Sowadski JM (1999) Crystal structure of the catalytic subunit of c-AMP-dependent protein kinase complexed with Mg/ATP and peptide inhibitor. Biochemistry 32:2154–2161